Journal of Catalysis **206,** 281–294 (2002)
doi:10.1006/jcat.2001.3482, available online at http://www.idealibrary.com on IDEAL®

Effects of Copper on the Catalytic Properties of Bimetallic Pd–Cu/(Ce,Zr)O_x/Al_2O_3 and Pd–Cu/(Ce,Zr)O_x Catalysts for CO and NO Elimination

A. B. Hungría,* A. Iglesias-Juez,* A. Martínez-Arias,*,[1] M. Fernández-García,* J. A. Anderson,† J. C. Conesa,* and J. Soria*

*CSIC, Campus Cantoblanco, Instituto de Catálisis y Petroleoquímica, 28049 Madrid, Spain; and †Department of Chemistry, University of Dundee, DD14HN, Scotland, United Kingdom

Received August 16, 2001; revised November 21, 2001; accepted November 23, 2001

A series of Pd–Cu bimetallic catalysts supported on Ce–Zr mixed oxide or on (Ce,Zr)O_x/Al_2O_3 mixed supports (with loadings of 10 and 33 wt% Ce–Zr mixed oxide) have been examined and compared to reference monometallic catalysts to determine the influence of copper on the catalytic activity for CO oxidation and NO reduction using a mixture of either O_2 or O_2–NO as oxidant under stoichiometric conditions. The samples were characterized by X-ray diffraction, transmission electron microscopy–X-ray energy-dispersive spectrometry, and electron paramagnetic resonance, employing *in situ* diffuse reflectance Fourier transform spectroscopy and X-ray absorption near-edge spectroscopy techniques to characterize physicochemical processes taking place during the course of the reactions. All the catalysts show Ce–Zr mixed oxide nanoparticles with pseudocubic phases and a Ce/Zr atomic ratio close to 1. The main differences between the samples are attributed to changes in the distributions of the two metallic components over the supports. The beneficial effects of copper on the catalytic activity of alumina-containing samples are related to the formation of an active Pd–Cu alloy in contact with the Ce–Zr mixed oxide component. A preferential interaction between copper and alumina in these samples is proposed to optimize the properties of the alloy phase by decreasing the copper concentration in the latter. However, the destruction of the alloy under reaction conditions at high temperatures, required for NO activation, removes the copper-promoting effects for NO reduction. The catalytic behavior of the Pd–Cu/(Ce,Zr)O_x sample is governed by the Cu–(Ce,Zr)O_x character of its active sites, which induces both beneficial and detrimental effects, on its catalytic properties, depending on the type of reaction.

Key Words: **Pd–Cu bimetallic catalysts; Pd–Cu alloy; CeO_2–ZrO_2; Al_2O_3; CO oxidation; NO reduction; XRD; TEM–XEDS; Cu^{2+}-EPR; *in situ* DRIFTS; *in situ* XANES.**

1. INTRODUCTION

Three-way catalysts (TWC) have been widely used to diminish pollutant emissions from gasoline-engine-powered vehicles (1). The classical components of these systems usually include Rh, Pt, and/or Pd as active metals, ceria as promoter, and high-surface alumina as the support (1, 2). More recently, the classical promotion by ceria was extended to other oxide systems to increase or maintain the durability of the TWC while decreasing the toxic emissions produced during the cold-start (or light-off) period, which may represent a considerable portion of the total emissions produced during any driving cycle (1, 3). Ce–Zr mixed oxide systems have been considered as potential substitutes to ceria on the basis of their greater oxygen storage capacity (OSC) after thermal sintering, which could potentially decrease the cold-start emissions mainly by allowing the catalyst to be located in positions closer to the engine manifolds with minimum system deactivation being produced (4). A certain degree of controversy exists with respect to the optimum configuration (Al_2O_3-supported or unsupported) of the Ce–Zr mixed oxide component in these catalysts (5). This controvery is mainly due to the difficulties experienced when preparing the alumina-supported materials. These are stabilized upon formation of nanosized particles (4, 6), achieving their catalytically optimal configuration for Ce/Zr atomic ratios close to 1 and upon formation of mixed oxide pseudocubic structures. Promising results were obtained by employing synthesis methods based on the use of reverse microemulsions (6, 7) in contrast to more classical methods based on coimpregnation (4, 8, 9). On the other hand, uncertainties exist concerning the formation of adequate interactions between the noble metals and the mixed oxide component in the alumina-supported configuration (5), although recent catalytic activity results have suggested the optimum performance of this configuration under stoichiometric $CO + O_2 + NO$ gas mixtures (10). Additionally, a higher OSC was achieved for (Ce,Zr)O_x/Al_2O_3 materials in comparison to unsupported (Ce,Zr)O_x or CeO_2/Al_2O_3 systems (9, 11).

The use of Pd as the only active metal component in TWC has received considerable attention on the basis of

[1] To whom correspondence should be addressed. Fax: 34 915854760. E-mail: amartinez@icp.csic.es.

0021-9517/02 $35.00

economical aspects (the high cost and scarcity of Rh), the availability of cleaner fuels, and its remarkable activity in oxidation reactions (1, 12). However, some limitations are apparent for Pd-only systems with respect to their performance in NO reduction reactions (12–14). In this sense it would be desirable to promote Pd with lower cost base metals instead of using Rh as an additional active metal, despite the latter's well-known activity for NO elimination (15). In this respect, promising results were obtained by using Mn, Cr, or Cu, which have been attributed either to the formation of the corresponding alloys (with consequent perturbation of the Pd electronic properties) or, in the case of Mn, to a mixture of effects involving alloy formation and Pd–MnO_x interactions (16–18). In the case of copper, the promoting effect induced upon alloying on both CO oxidation and NO reduction activities may be explained, according to theoretical studies (19), by the strong modification produced in the Pd valence state upon charge injection into the *sp* sub-band. This beneficial effect of Pd–Cu alloy formation under stoichiometric $CO + O_2 + NO$ was experimentally demonstrated over a Pd–Cu/CeO_2/Al_2O_3 catalyst (18).

In this work, following a preliminary report on these systems (20), we extend the study of a ceria-promoted Pd–Cu catalyst (18) to similar systems promoted in this case by a Ce–Zr mixed oxide, with a focus on determining which main parameters affect the catalytic performance in the reactions of interest for the TWC. A series of Pd–Cu bimetallic catalysts, supported on either Ce–Zr mixed oxide or (Ce,Zr)O_x/Al_2O_3 mixed supports with different mixed oxide loadings, were studied by a multitechnique approach using X-ray diffraction (XRD), transmission electron microscopy–X-ray energy-dispersive spectrometry (TEM–XEDS), and electron paramagnetic resonance (EPR) for catalyst characterization, and by using catalytic activity in combination with *in situ* diffuse reflectance Fourier transform spectroscopy (DRIFTS) and X-ray absorption near-edge spectroscopy (XANES) techniques to evaluate the catalytic performance and the physicochemical processes which take place during the course of stoichiometric $CO + O_2$ or $CO + O_2 + NO$ reactions over the catalysts.

2. EXPERIMENTAL

2.1. Catalyst Preparation

Two ceria–zirconia/alumina supports, 10 and 33 wt%, of mixed oxide—expressed as $Ce_{0.5}Zr_{0.5}O_2$—(10CZA and 33CZA; $S_{BET} = 186\ m^2\ g^{-1}$ and $S_{BET} = 164\ m^2\ g^{-1}$, respectively) were prepared by modifying the microemulsion method used previously for preparing the unsupported oxide (CZ; $S_{BET} = 96\ m^2\ g^{-1}$) (6). Full details of the procedure can be found elsewhere (7). After drying overnight at 373 K these supports were calcined under air at 773 K for 2 h. According to inductively coupled plasma–atomic emission spectroscopy (ICP–AES) chemical analysis, the two CZA and the CZ samples have Zr/Ce atomic ratios of 1.0 ± 0.1 (6, 7). The three supports (10CZA, 33CZA, and CZ) were coimpregnated (incipient wetness method) with aqueous solutions of palladium and copper nitrates (from Alfa Aesar and Merck, respectively; purities >99.99%) to give 1.0 wt% metal loadings of each metal. The catalysts were calcined following the same drying/calcination procedure described previously for the supports. The catalysts are referred to as PdCu10CZA, PdCu33CZA, and PdCuCZ, corresponding to the systems supported on 10CZA, 33CZA, and CZ, respectively. Similar methods and materials were applied for the preparation of reference catalysts Pd10CZA, Pd33CZA, and PdCZ (with 1 wt% Pd on 10CZA, 33CZA, and CZ, respectively), CuA (1 wt% Cu on alumina), and CuCZ (1 wt% Cu on CZ).

2.2. Catalytic Tests

Catalytic tests using stoichiometric mixtures of 1% $CO + 0.5\%\ O_2$ or 1% $CO + 0.45\%\ O_2 + 0.1\%$ NO (N_2 balance) were performed at 30,000 h^{-1} in a Pyrex glass flow reactor system. Details of the experimental conditions employed for these tests can be found elsewhere (21). Gases were regulated with mass flow controllers and analyzed online using a Perkin–Elmer 1725X FTIR spectrometer coupled with a multiple reflection transmission cell (Infrared Analysis Inc.). Oxygen concentrations were determined using a paramagnetic analyzer (Servomex 540A). The experimental error in the conversion values obtained under these conditions was estimated as $\pm 7\%$. Prior to catalytic testing, *in situ* calcination was performed in diluted oxygen (2.5% O_2 in N_2) at 773 K, followed by cooling under the same atmosphere and a N_2 purge at room temperature (RT). A typical test consisted of increasing the temperature from 298 to 823 K at 5 K min^{-1}.

2.3. Characterization Techniques

Powder XRD patterns were recorded on a Siemens D-500 diffractometer using nickel-filtered Cu$K\alpha$ radiation operating at 40 kV and 25 mA with a 0.025° step size.

TEM experiments were carried out using a JEOL 2000 FX (0.31 nm point resolution) equipped with a LINK (AN 10000) probe for XEDS analysis. The sample spot for XEDS analysis was in the 50–100 nm range. Portions of samples were crushed in an agate mortar and suspended in butyl alcohol. After ultrasonic dispersion, a droplet was deposited on a nickel grid supporting a perforated carbon film. Micrographs, electron diffractograms, and, where necessary, dark-field images were recorded over selected areas with compositions previously characterized by XEDS. Six to 10 aggregates of a typical size of 200–300 nm were studied for each sample, using TEM–XEDS to analyze about two to four different zones of each aggregate.

Electron paramagnetic resonance (EPR) spectra were recorded at 77 K with a Bruker ER 200 D spectrometer operating in the X-band and calibrated with a α,α'-diphenyl-β-picrylhydrazyl (DPPH) standard ($g = 2.0036$). Portions, between 20 and 40 mg, of the sample were placed inside a quartz probe cell with greaseless valves and pretreated with 300 Torr of pure O_2 at 773 K, followed by thorough outgassing at room temperature.

DRIFTS analysis of adsorbed species present on the catalyst surface under reaction conditions was carried out using a Perkin–Elmer 1750 FTIR spectrometer fitted with an MCT detector. Analysis of the NO conversion at the outlet of the IR chamber was performed by chemiluminescence (Thermo Environmental Instruments 42C). The DRIFTS cell (Harrick) was fitted with CaF_2windows and a heating cartridge that allowed samples to be heated to 773 K. Samples of ca. 80 mg were calcined *in situ* at 773 K (with synthetic air −20% O_2 in N_2-) and then cooled to 298 K in synthetic air before introducing the reaction mixture and heating at 5 K min^{-1} up to 673 K, recording one spectrum (4 cm^{-1} resolution, average of 20 scans) generally every 10–15 K. The gas mixture (using the same concentrations as those employed for laboratory reactor tests) was prepared using a computer-controlled gas blender with 75 cm^3 min^{-1} passing through the catalyst bed.

XANES experiments at the Ce L_{III}- and Pd K-edges were performed at line EXAFS-IV of the DCI synchrotron at LURE. A Si(311), (for Ce) or Ge(400) (for Pd) double-crystal monochromator was used in conjunction with a rejection mirror to minimize the harmonic content of the beam. Transmission experiments were carried out using N_2/O_2- or Ar-filled ionization chambers. The energy scale was simultaneously calibrated by measuring a CeO_2 wafer or Pd foil which was inserted before a third ionization chamber. Samples were self-supported (absorbance 0.5–2.0) and placed in a controlled-atmosphere cell for treatment. XANES spectra were taken every 15 K in the presence of the $CO + NO + O_2$ flowing mixture (similar to the mixture employed for catalytic activity tests) during a 5 K min^{-1} temperature ramp up to 623 K. The series of spectra were analyzed by using a statistical method called principal factor analysis, details of which can be found in (22).

3. RESULTS

3.1. XRD and TEM–XEDS

XRDs of the Ce–Zr mixed oxide-promoted bimetallic catalysts are shown in Fig. 1 and show peaks arising from both the γ-Al_2O_3 support and the Ce–Zr (CZ) mixed oxide component. The latter are indexed in the cubic F*m*3*m* space group. They show a decreasing linewidth with increasing the CZ concentration and are barely discernible in the PdCu10CZA sample. An analysis of the lattice parameters, which employ the most intense (111) reflection of CZ, and

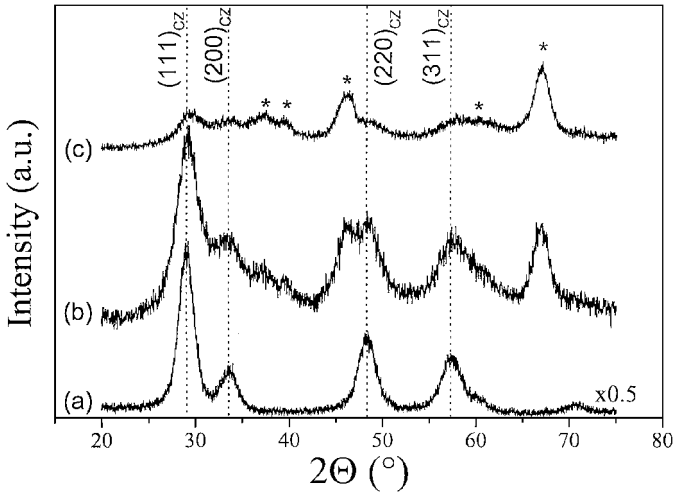

FIG. 1. X-ray diffractograms of (a) PdCuCZ, (b) PdCu33CZA, and (c) PdCu10CZA. The main reflections of the CZ cubic phase are marked. Peaks marked with an asterisk correspond to alumina-related diffractions.

a comparison to literature results obtained over a series of Ce–Zr mixed oxides with different Ce/Zr atomic ratios (4) are in agreement with the formation of a $Ce_xZr_{1-x}O_2$ phase in all cases. This shows a Ce/Zr atomic ratio ≈1 for PdCu10CZA and PdCuCZ, but a slight cerium enrichment, corresponding approximately to an average-composition $Ce_{0.6}Zr_{0.4}O_2$ for PdCu33CZA. This indicates that some of the zirconium is not detected by diffraction in the latter sample, as has been shown to occur in other Al_2O_3-supported Ce–Zr mixed oxide samples (4, 8).

Figure 2 shows the radial densitometries extracted from electron diffraction experiments which show maxima or

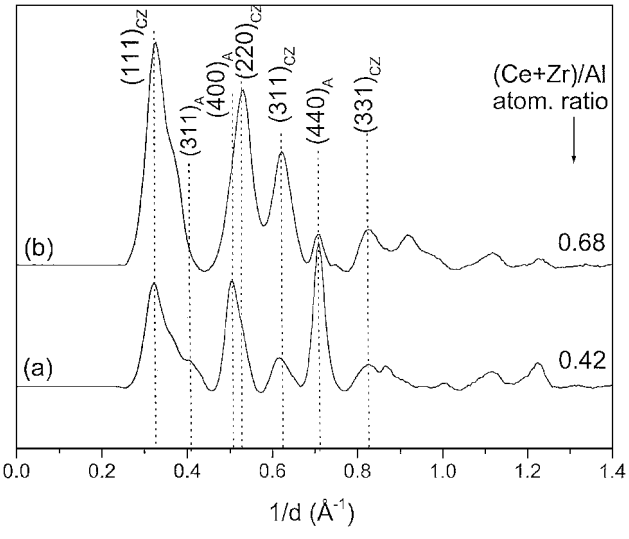

FIG. 2. Radial (angle-averaged) densitometry patterns of the electron diffraction rings observed in specific zones of (a) PdCu10CZA and (b) PdCu33CZA. Vertical dotted lines mark the strongest reflections attributed to Ce–Zr mixed oxide and alumina-related phases (subscripted as CZ and A, respectively).

TABLE 1

Summary of XRD and TEM/ED/XEDS Results

Samples	Cell parameter (Å)	Average particle size (nm)[a]	$(Ce/Zr)_{at.\ ratio}$[b]	$(Ce+Zr/Al)_{at.\ ratio}$[b,c]
PdCu10CZA	5.30[d]	2	0.8–1.2	0.25–0.46
PdCu33CZA	5.32[d]	3	0.3–1.6	0.2–1.8
PdCuCZ	5.30[d], 5.29[e]	5	0.9–1.2	—

[a] Obtained from dark-field TEM images using the (111) ring of $Ce_xZr_{1-x}O_2$.
[b] XEDS results.
[c] Only zones presenting detectable amounts of Ce,Zr are included.
[d] From electron diffraction results.
[e] From XRD results.

shoulders that are assigned, in accordance with XRD results, to the most prominent diffractions of the previously mentioned cubic phase of the Ce–Zr mixed oxide and of γ-Al_2O_3. No evidence was obtained regarding the existence of Pd- or Cu-containing phases in these experiments in any of the regions analyzed, indicating that the catalysts presented a relatively high metal dispersion. The stability of the samples under reaction conditions was verified by performing X-ray or electron diffractograms on the samples, after their use in catalytic reaction, which show the same features as those observed for the initial fresh catalysts. The data obtained from XEDS analysis of different zones of the samples and the main structural and geometrical characteristics obtained for the CZ component by XRD and TEM–XEDS experiments are summarized in Table 1. It may be noted that in accordance with the linewidths observed by X-ray or electron diffraction (Figs. 1 and 2), the particle size increases with the amount of CZ, although moderate sizes, mainly resulting from the particular characteristics of the preparation method employed (7), are present in all cases.

Some information about the palladium distribution on the samples was obtained by XEDS analysis (Fig. 3). Unfortunately, it was not possible to perform an analogous study for copper due to the presence of this element in the sample holder of the microscope. Analysis of the data displayed in Fig. 3 shows that Pd appears irregularly distributed over the supports appearing mainly in zones enriched in Ce–Zr for both PdCuxCZA samples, particularly for the sample with higher CZ loading.

3.2. EPR

EPR spectra of the calcined Pd–Cu catalysts along with that of the reference CuA sample are shown in Fig. 4. The spectrum of CuA (Fig. 4a), which was analyzed in detail in a previous contribution (23), is composed of two overlapping Cu^{2+} signals. The first signal, which contributes to roughly 20% of the doubly integrated intensity of the spectrum, displays axial shape with $g_\parallel = 2.321$ and $g_\perp = 2.057$ showing resolved hyperfine patterns of four lines in each of its components with $A_\parallel = 17.1 \times 10^{-3}$ cm^{-1} and $A_\perp = 1.9 \times 10^{-3}$ cm^{-1}. This can be assigned to isolated Cu^{2+} ions with a tetragonally distorted octahedral symmetry (23, 24). The major signal does not show resolved hyperfine splittings and exhibits an anisotropic (quasiaxial) lineshape with extremes at $g_\parallel = 2.24$ and $g_\perp = 2.05$. On the basis of its EPR parameters and the absence of hyperfine splitting resolution, this can be generically assigned to clustered Cu^{2+} ions belonging to an oxidic phase, probably of the $CuAl_2O_4$ type (23, 25). Double integration of the spectrum and comparison with a copper sulfate standard show

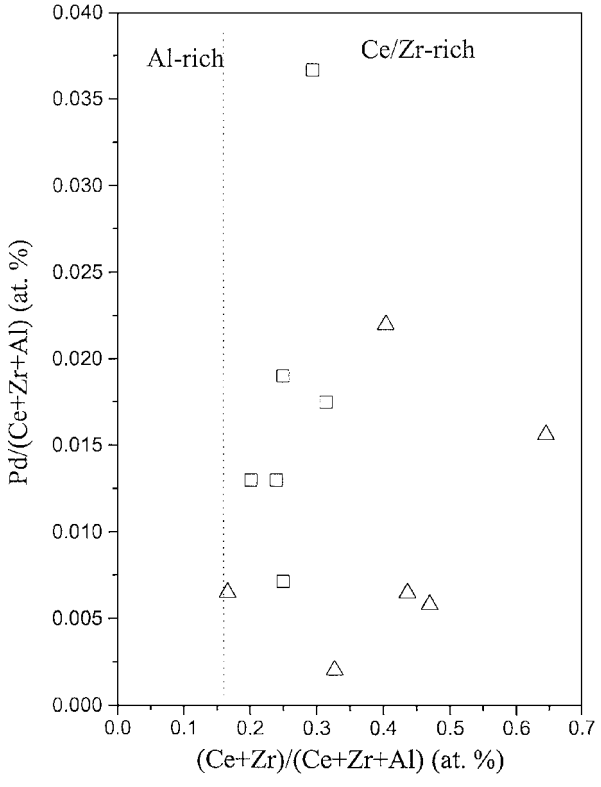

FIG. 3. XEDS data obtained for PdCu10CZA (squares) and PdCu33CZA (triangles). Dashed vertical line is used only as a guide.

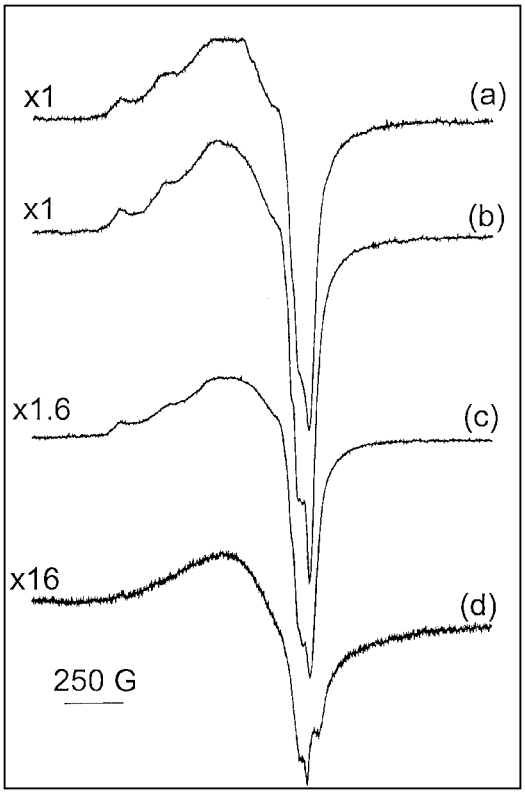

FIG. 4. EPR spectra at 77 K of initial calcined samples. (a) CuA, (b) PdCu10CZA, (c) PdCu33CZA, and (d) PdCuCZ.

that about 55% of the total copper content is detected in this spectrum (Fig. 4a). A considerably smaller amount of the total copper (19.5%) appears as EPR detectable species in the spectrum of PdCuCZ (Fig. 4d), which is composed of two overlapping Cu^{2+} signals similar to those observed in previous studies of CuCZ (26). The first signal, attributable to Cu^{2+} ions in small copper oxide clusters (26, 27), predominates in the spectrum and shows unresolved hyperfine splitting and anisotropic (quasiaxial) lineshape with extremes at $g_{\parallel} = 2.20$ and $g_{\perp} = 2.04$. The second signal, attributable to isolated Cu^{2+} ions in tetragonally distorted octahedral symmetry (26, 27), makes a very minor contribution to the spectrum. This results in its poor definition, resolving only its most prominent hyperfine perpendicular features at $g_{\perp} = 2.036$ and $A_{\perp} = 1.8 \times 10^{-3}$ cm^{-1}. The spectra observed for PdCu10CZA and PdCu33CZA (Figs. 4b and 4c) are similar to that observed for CuA both in terms of the signals present and in terms of the amount of Cu^{2+} species detected in them (63.1 and 43.5% of the total copper content for PdCu10CZA and PdCu33CZA, respectively). This suggests that the larger contributions to the spectra correspond to Cu^{2+} species in contact with the alumina component of the samples. The presence of small amounts of Cu^{2+} species in contact with the CZ mixed oxide, which increase with the loading of this component, is suggested by both the slight shift of the maximum of the spectra (appearing in the central part of them) toward a higher magnetic field and the presence of the most prominent hyperfine perpendicular feature at $g \approx 2.03$, characteristic of these species, as indicated by comparison to the spectrum of PdCuCZ (Fig. 4d).

3.3. *Catalytic Activity Tests*

Conversion profiles for the bimetallic catalysts in the $CO + O_2$ and $CO + O_2 + NO$ reactions are shown in Fig. 5. Important differences are observed in the catalytic performances as a function of changes in the support composition and the presence of NO in the feed stream. Thus, while the efficiency for CO oxidation in the absence of NO decreases in the order PdCu33CZA > PdCu10CZA > PdCuCZ (Fig. 5, top), in the presence of

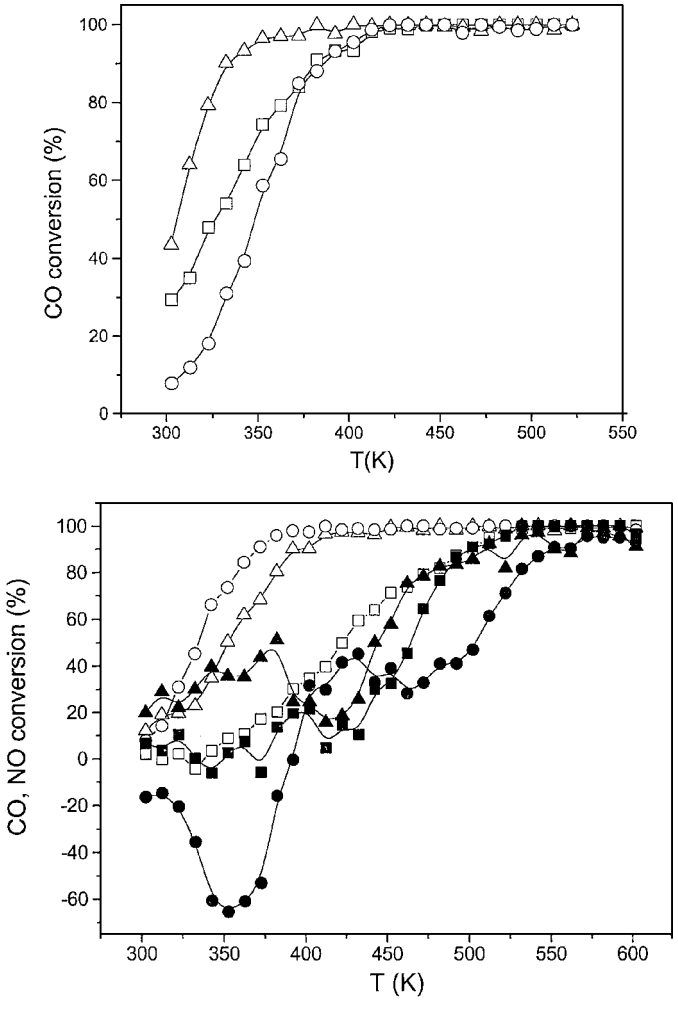

FIG. 5. Top: Conversion profiles for the $CO + O_2$ reaction over PdCu10CZA (squares), PdCu33CZA (triangles), and PdCuCZ (circles). Bottom: As above for the CO–O_2–NO reaction. Open symbols, CO conversion; full symbols, NO conversion.

TABLE 2

Fifty Percent Isoconversion Temperatures (T_{50}, K) Observed for the Bimetallic and Monometallic Reference Catalysts in the $CO + O_2$ and $CO + O_2 + NO$ Reactions at 30,000 h^{-1}[a]

	PdCu10CZA	PdCu33CZA	PdCuCZ	Pd10CZA	Pd33CZA	PdCZ	CuCZ
T_{50} (CO conv.) ($CO + O_2$)	327	306	346	404	383	<303[b]	387
T_{50} (CO conv.) ($CO + O_2 + NO$)	424	354	336	433	377	358	380
T_{50} (NO conv.) ($CO + O_2 + NO$)	466	445	503	456	442	485	534

[a] Complete conversion profiles for the reference monometallic catalysts are available in Refs. (10) and (21) (Pd10CZA, Pd33CZA, and PdCZ in $CO + O_2$ and $CO + O_2 + NO$ reactions, respectively) and (26) and (40) (CuCZ in $CO + O_2$ and $CO + O_2 + NO$ reactions, respectively).

[b] Conversion, 100%, is achieved from the initial temperature (303 K), giving rise to a ca. 30 K temperature increase (as a consequence of the exotherm), and maintained throughout the test.

NO it decreases monotonically with decreasing the CZ loading (Fig. 5, bottom). A comparison of the CO conversion profiles in the presence and absence of NO reveals that while CO oxidation over CZA-supported catalysts is significantly deactivated by NO, PdCuCZ is almost unaffected, or slightly enhanced (see Table 2), by this reactant. On the other hand, NO reduction activity follows the order PdCu33CZA > PdCu10CZA > PdCuCZ. It is also worth noting that significant NO desorption, producing negative conversion values, is produced at temperatures below ca. 370 K for PdCuCZ. A comparison to data for the reference monometallic catalysts (Table 2) shows the promoting effect of copper in CO oxidation for both reactions, with the exception of PdCuCZ in the $CO–O_2$ reaction. In contrast, NO reduction is slightly deactivated by the presence of copper in the CZA-supported catalysts and to a greater extent in the CZ-supported system. It is worth noting that, like in the case of PdCuCZ, a slight enhancement in catalytic activity for CO oxidation is observed in the presence of NO for CuCZ. It may be also observed that this CuCZ catalyst, which may be assumed on the basis of comparison to a similar series of CeO_2- and CeO_2/Al_2O_3-supported copper catalysts (28), to be the most active for CO oxidation among monometallic copper catalysts for either a CZ or a CZA series of supported catalysts, shows a poorer CO oxidation performance than its homologous PdCuCZ.

3.4. In Situ DRIFTS

Spectra in the carbonyl stretching region for the three Pd–Cu catalysts during the $CO + O_2$ reaction are shown in Figs. 6A to 6C. A reasonable correlation can be observed for all samples between the evolution of bands due to gaseous CO (barely discernible due to overlapping with bands adsorbed carbonyl species, in the 2200–2050 cm^{-1} range) and CO_2 (2400–2300 cm^{-1}), and the CO conversion profiles presented in Fig. 5. In general terms, complex spectra are observed resulting from the overlapping of different carbonyl species due to adsorption on exposed palladium or copper entities (in different oxidation states). Under these conditions, the analysis of the evolution and the assignment of the different bands observed are made mainly on the basis of previous results obtained using similar monometallic systems (of both Pd and Cu) treated under similar conditions (10, 21, 26, 29).

For the three samples, a band at ca. 2110 cm^{-1} appeared immediately upon contact with the reactant mixture and was of particularly high intensity for PdCuCZ in which it largely dominated the spectra. This band shows maximum intensity at intermediate, relatively low, reaction temperatures, and it showed a slight red shift concomitant with a decrease in intensity with increasing reaction temperature. This band is similar to a band observed for the CuCZ reference catalyst treated under similar conditions (26) and, consistent with the observation of its greatest intensity for PdCuCZ, it arises from carbonyl species adsorbed on Cu^+ ions at sites located at the copper oxide–CZ interface, which are readily created by reductive interaction with CO (26, 27). Another band appearing at 2117 cm^{-1} for PdCu10CZA may be attributed to adsorbed carbonyls on Cu^+ sites in contact with the alumina surface (23).

A band at ca. 1970 cm^{-1}, due to bridging carbonyl species adsorbed on Pd^0 surfaces (10, 21, 29, 30), is also apparent for the three samples upon contact with the reactant mixture, showing maximum intensity at intermediate reaction temperatures, and was slightly red-shifted (as a consequence of decreasing CO coverage (10, 21, 29, 30)) for temperatures above this maximum. It is worth noting that the species giving rise to this band are developed less readily with reaction temperature for the PdCuCZ sample than either the other two samples or the monometallic PdCZ sample (21). A band (or shoulder) at 2096–2063 cm^{-1}, due to linearly adsorbed carbonyls on Pd^0 (10, 21, 29, 30), may be also be distinguished for PdCuxCZA samples at $T \geq$ ca. 323 K and shows a red shift with an increasing reaction temperature which was more pronounced than that for the bridging carbonyls. This can be attributed to a decrease in the CO coverage on the palladium particles, with the greatest shift observed for the linear carbonyls being related either

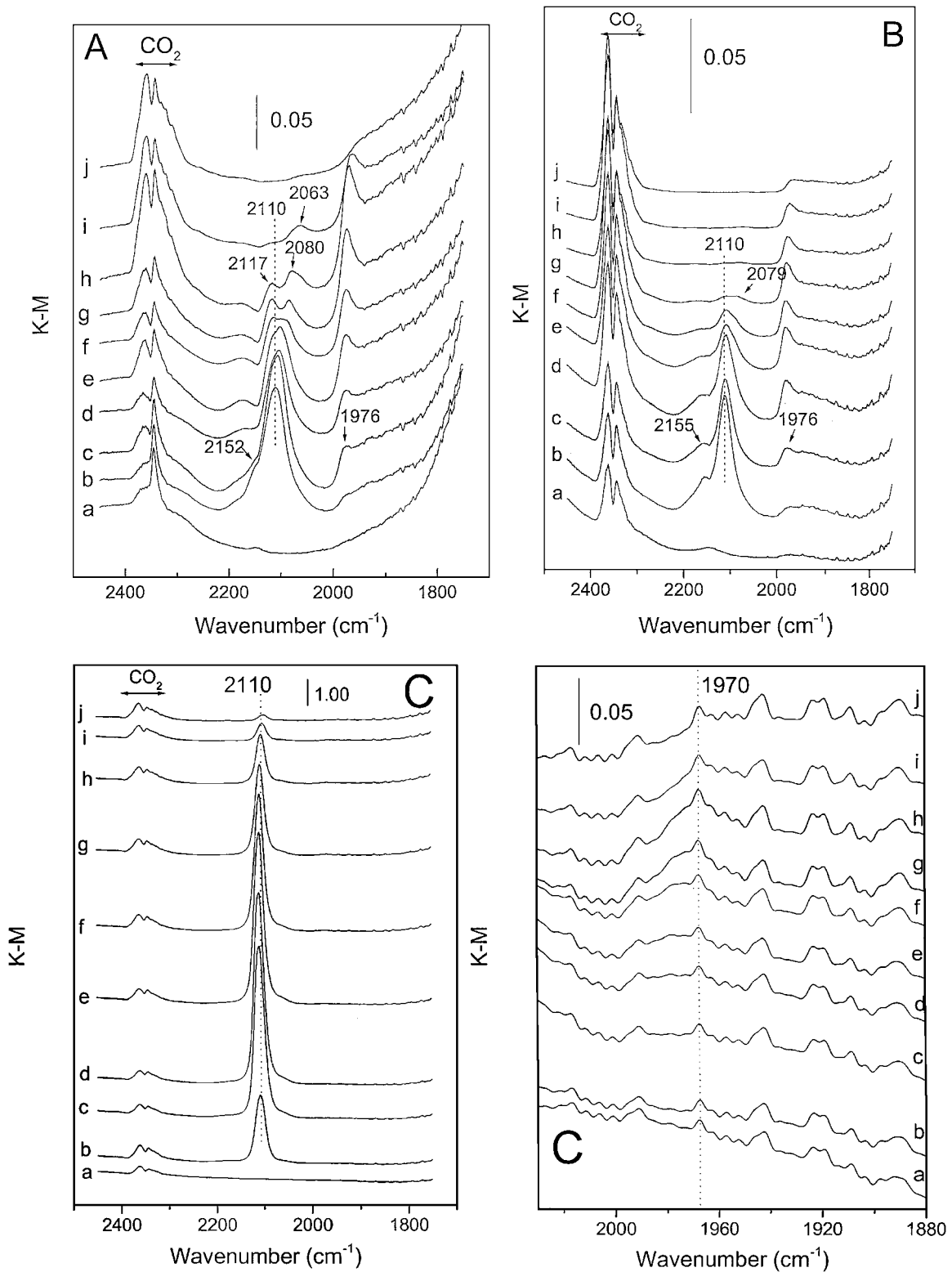

FIG. 6. *In situ* DRIFTS spectra for (A) PdCu10CZA, (B) PdCu33CZA, and (C) PdCuCZ (showing a detail of the 2030–1880 cm^{-1} zone) catalysts. (a) Before introduction of the reactant mixture. Recorded under 1% CO and 0.5% O_2 at the following temperatures: (b) 303, (c) 323, (d) 343, (e) 363, (f) 383, (g) 403, (h) 423, (i) 443, and (j) 463 K.

to their lower adsorption energy (30), thus greater ease of desorption, or to the greater activity of the centers where the palladium particles are adsorbed. Considering the high sensitivity in the frequency of the linear carbonyls adsorbed on the Pd^0 to CO coverage, one cannot fully dismiss the fact that these species are already formed for PdCuxCZA upon contact with the reaction mixture at RT, as observed for monometallic Pd catalysts (21), which in this case are obscured by the strong overlapping band of Cu^+ carbonyls at 2110 cm^{-1}. The previous observation is true at any reaction temperature for PdCuCZ. Other bands which, on the basis of results for the monometallic Pd series (21), can be attributed to Pd carbonyls are those at 2155–2152 cm^{-1}, which appear at relatively low temperatures and are attributed to adsorption at Pd^{2+} sites (21, 31).

To examine the state of the surface on completion of the runs (under $CO–O_2$ up to 473 K) in the absence of reaction- or thermal desorption-derived effects, the samples were cooled under N_2 to room temperature and then exposed to 1% CO in N_2 before flushing the cell with N_2. Spectra recorded under these conditions are shown in Fig. 7. A band at 1980 cm^{-1} due to bridging carbonyls adsorbed on Pd^0 particles was observed for all three samples. Additionally, linear carbonyls on the Pd^0 particles were also detected as a band or shoulder at ca. 2099 cm^{-1} for the PdCuxCZA samples. The presence of these carbonyls could not be discerned, however, for PdCuCZ; this may be due to the strong absorption band of Cu^+ carbonyls at 2110 cm^{-1}. This latter band was also observed, but with a significantly lower intensity, for PdCu33CZA and might also be present for PdCu10CZA, although this was not possible to confirm due to overlapping with other bands in that region. PdCu10CZA also exhibited a band at 2117 cm^{-1} due to Cu^+ carbonyls.

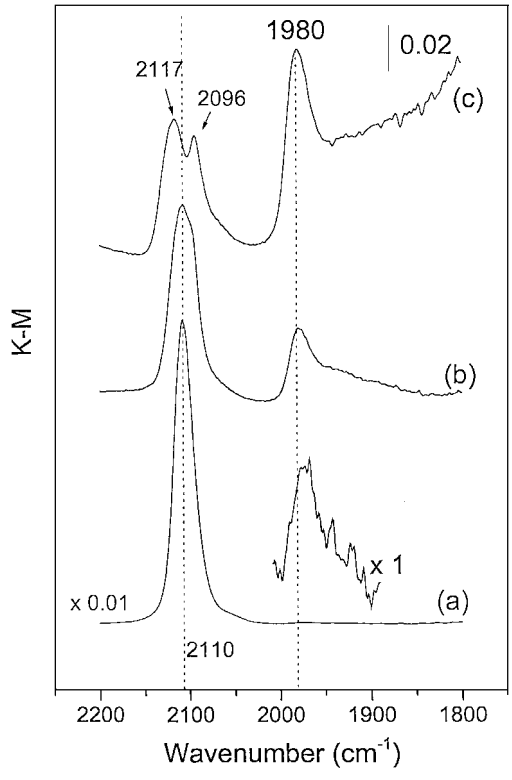

FIG. 7. DRIFTS spectra obtained following experiments shown in Fig. 6, by cooling under a flow of N_2 and admission of CO at room temperature and flushing with N_2 for (a) PdCuCZ, (b) PdCu33CZA, and (c) PdCu10CZA.

Spectra recorded under $CO–O_2–NO$ reaction conditions for the three Pd–Cu samples are shown in Figs. 8A–8C. Carbonyl bands with a similar nature to those observed under $CO–O_2$ were observed in all cases. The three samples displayed bands in the 2120–2110 cm^{-1} range due to carbonyl species adsorbed on Cu^+. Significantly, the band for PdCuCZ was of appreciably lower intensity than that under $CO–O_2$ and appeared at slightly higher wavenumbers at the lower reaction temperatures. Other differences, when compared to the experiments performed under $CO–O_2$, concern the relatively higher stability of Pd^{2+} carbonyls (appearing at 2158–2155 cm^{-1}) observed for the PdCuxCZA samples in the presence of NO. It is of note that these bands were not detected for PdCuCZ (Fig. 8C). Additionally, bands due to carbonyl species adsorbed on Pd^0 had a relatively lower overall intensity in the presence of NO and developed to a lesser extent with increasing reaction temperature. Additional bands at 2250 and 2232 cm^{-1}, not detected in the absence of NO, were observed in the spectra of PdCuxCZA samples from ca. 423 to 453 K for PdCu10CZA and PdCu33CZA, respectively. These species are assigned to isocyanate species adsorbed on octahedral and tetrahedral Al^{3+} cations, respectively (32), and result from NO dissociation followed by N–CO combination on the metallic particles and spillover of the NCO species onto the alumina support (32). An additional band at 1874 cm^{-1}, only observed for PdCuCZ, is attributed to nitrosyl species adsorbed on Cu^{2+} cations (33–35).

Postreaction experiments similar to those shown in Fig. 7 were recorded after the runs under $CO–O_2–NO$ (Fig. 9). The main differences between these spectra and those observed after the $CO–O_2$ reaction involve the presence of a shoulder at ca. 2150 cm^{-1} for PdCu33CZA and with a lower intensity for PdCu10CZA, which indicates the presence of carbonyls adsorbed at Pd^{2+} sites. On the other hand, the nature and intensity of Pd^0 carbonyls (bridging species at 1985–1981 cm^{-1} detected for the three samples and linear carbonyls detected as shoulders at ca. 2094 cm^{-1} for PdCuxCZA samples) appear roughly similar to those detected after the runs under $CO–O_2$ (Fig. 7). Greater differences between both experiments involve Cu^+-related carbonyls (bands at 2119–2110 cm^{-1}), which show relatively higher intensities in the experiments performed after the $CO–O_2–NO$ runs and appear slightly blue-shifted for the PdCuxCZA samples.

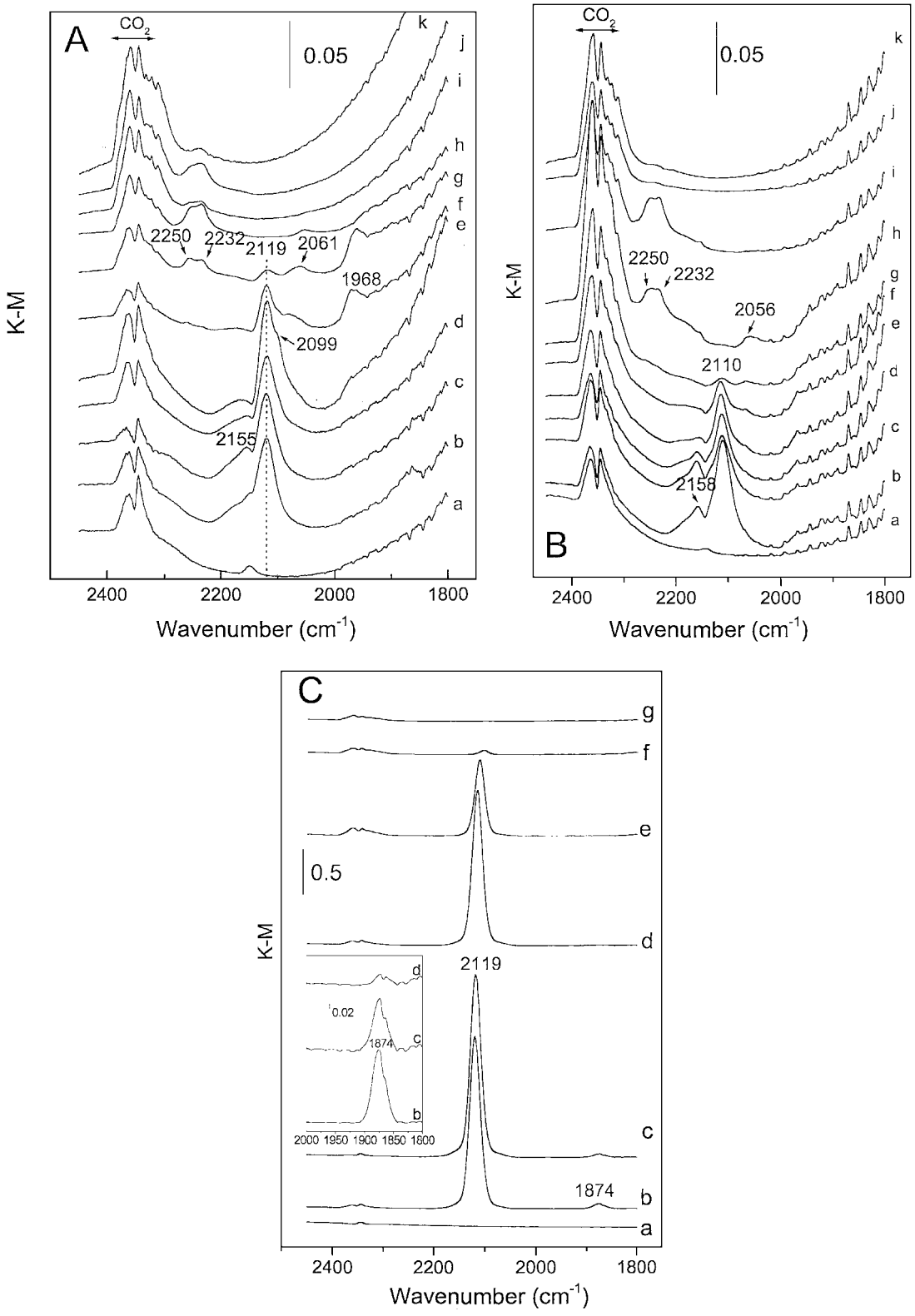

FIG. 8. *In situ* DRIFTS spectra for (A) PdCu10CZA, (B) PdCu33CZA, and (C) PdCuCZ (the 2000–1800 cm^{-1} zone is shown expanded in the inset) catalysts. (a) Before introduction of the reactant mixture. Recorded under 1% CO, 0.45% O_2, and 0.1% NO at the following temperatures: (b) 303, (c) 333, (d) 363, (e) 393, (f) 423, (g) 453, (h) 483, (i) 513, (j) 543, and (k) 573 K.

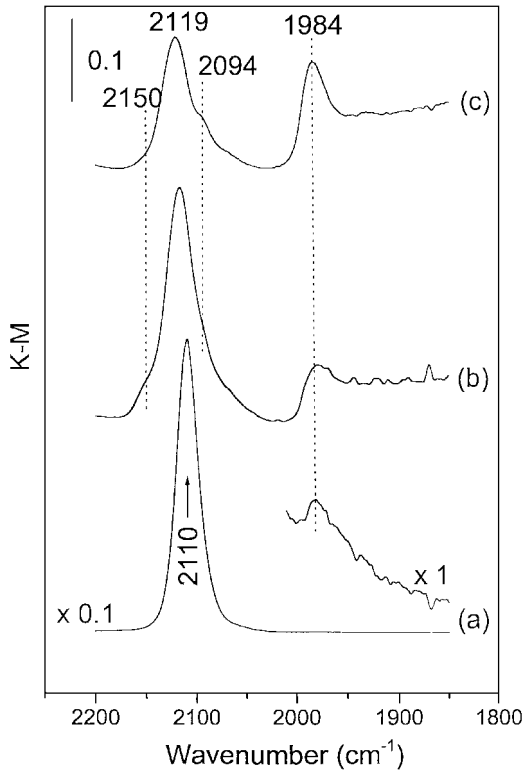

FIG. 9. As for Fig. 7, following the experiments of Fig. 8.

3.5. *In Situ XANES*

Factor analysis results at the Pd K-edge, obtained during a temperature-programmed reaction run under CO–O_2–NO for PdCu33CZA, are consistent with the existence of three different chemical species displaying the absorption spectra exhibited in Fig. 10. From a comparison to XANES spectra of reference compounds (36), components 1 and 2 are identified as oxidized species with a local geometry similar to that of PdO (D_{2h} symmetry) and a reduced species with metal-like character, respectively, while component 3 is attributed to a Pd–Cu alloy. Metallic-like Pd appears to have a depleted 5*sp* population (resonance at ca. 24,365 eV), as was shown to occur with the monometallic sample (10), while the Pd–Cu alloy XANES spectrum displays the typical characteristics of such a phase: a significant number of 5*sp* holes and a strong modification of Pd f-final states (resonance at ca. 24,385 eV) (36). An analysis of their concentration profiles through the reaction coordinate (Fig. 10) indicates that the reduced species developed from ca. 400 K, with full reduction being achieved at $T \geq 530$ K. The reduction process yields metallic Pd (from ca. 400 K) which is partially transformed to the Pd–Cu alloy from ca. 440 K. This initial detection of Pd^0 and posterior existence of the Pd–Cu alloy may be interpreted on the basis that palladium interacts mainly with the CZ component, while copper interacts mainly with the alumina component; this would indicate that Pd^0 formation and mobility are required to yield alloy formation. This alloy appears, however, to be unstable under reaction conditions showing maximum concentration at ca. 500 K and reverting to metallic Pd at higher reaction temperatures.

4. DISCUSSION

4.1. *Characterization of the Pd–Cu Catalysts*

XRD and TEM–XEDS analyses of the characteristics of the CZ component reveal (Figs. 1 and 2, and Table 1) the presence of Ce–Zr mixed oxide with Ce/Zr ratios close to 1 for PdCu10CZA and PdCuCZ and with a slight cerium enrichment for PdCu33CZA. It must be noted that previous Raman characterization of the supports indicates that the cubic phase of the CZ component detected by the diffraction techniques most likely corresponds to a pseudo-cubic ($c/a = 1$, i.e., Ce and Zr cations remain in cubic positions) t'' phase with an overall tetragonal symmetry ($P4_2/nmc$ space group) arising from the displacement of oxide anions (6, 7). According to the literature, a metastable tetragonal phase t' (corresponding to space group $P4_2/nmc$ and in principle distinguishable from phase t'' by diffraction techniques as it shows $c/a \neq 1$) is thermodynamically favored for the mixed oxide with Ce/Zr ratios close to 1 (4). Stabilization of the less thermodynamically stable phase t'' for these samples can be attributed to the relatively small sizes of the CZ particles (Table 1) achieved by employing the microemulsion synthesis method (4, 6, 7). As observed in a previous report on the CZA supports (7), analysis of XEDS data (Table 1) indicates that the heterogeneity of the CZ component is largely increased for PdCu33CZA. In any case, both CZA-supported samples present small CZ particle sizes, and only a moderate particle size increase (from 2 to 3 nm in terms of average values) is produced by the threefold increase in CZ loading. According to previous oxygen adsorption EPR studies on the CZA supports and the reference PdxCZA catalysts, the CZ component appears in two different configurations in the PdCuxCZA materials (7, 21): as three-dimensional particles (3D-CZ) and as two-dimensional patches (2D-CZ) dispersed on the alumina surface, the latter being undetectable by diffraction techniques. The relative amounts of these entities in the samples were indicated as being roughly proportional to the CZ loading on the basis of analysis of the relative intensities of superoxide entities formed on each (7, 21).

With respect to the metal components, XEDS and EPR results (Figs. 3 and 4) suggest that both Pd and Cu are irregularly distributed over the supports. Analysis of the XEDS data for Pd reveals a tendency to interact with the CZ mixed oxide component, which is less pronounced for PdCu10CZA, in the PdCuxCZA samples (Fig. 3). In this sample, it appears (Fig. 3) that Pd may present a more

homogeneous distribution. The opposite, i.e., a preference toward interaction with the alumina component as observed for CeO_2/Al_2O_3-supported copper catalysts (23, 28), is apparent for copper in the PdCuxCZA samples as suggested by the strong similarities observed in their EPR spectra when compared to that of CuA (Fig. 4). In turn, analysis of these spectra reveals that copper appears in different configurations, a minor portion as isolated Cu^{2+} species and a major one as clustered Cu^{2+} species in oxidic environments, which are most likely to be of a CuO-type nature for species interacting with CZ and of a $CuAl_2O_4$-type nature for species interacting with the alumina (23, 25, 26). In addition, a significant portion of the total copper, generally increasing with the amount of CZ mixed oxide present in the samples, forms species which are not detected by EPR. These may be attributed, on the basis of previous XPS experiments on samples of this type (26, 27), more to the presence of well-formed (most likely due to their relatively larger particle size in comparison with EPR-detectable clustered Cu^{2+}) oxidic phases of the CuO or $CuAl_2O_4$ type in which most of the Cu^{2+} are antiferromagnetically coupled (23, 27, 37) rather than to the presence of diamagnetic states of copper (like Cu^{+}).

4.2. Catalytic Activity for the CO–O_2 Reaction

Previous work on the catalytic activity for this reaction over the PdxCZA and PdCZ reference catalysts (see also Table 2) showed that the CZ promoter enhances the catalytic properties of the noble metal by favoring the formation of the metallic state and through generation of anionic vacancies (doubly ionized $V_{\ddot{o}}$ sites) in the CZ component at Pd–(3D-CZ) interface sites, which are the most active for the reaction (21). Both sites were created at room temperature for those catalysts (21), which facilitates CO and O_2 activation and opens up a new reaction pathway that circumvents the CO-inhibiting effects present in the absence of a promoter effect (2, 21, 29).

Data in Table 2 indicate a copper-promoting effect for the PdCuxCZA samples, the extent of which decreases with increasing CZ loading, while the presence of copper appears detrimental for the PdCuCZ catalyst. This behavior can be rationalized by considering the differences in the distribution of the two metallic components over the different supports. The lower activity of PdCuCZ (with respect to both PdCuxCZA and PdCZ samples and in contrast to the monometallic Pd catalysts (21)) suggests that active sites in this sample are located at copper–CZ interfaces, with copper exerting a kind of blocking effect on the most active Pd–CZ contacts (21). This hypothesis is supported by the presence of a very intense Cu^{+} carbonyl band at 2110 cm^{-1} (Fig. 6C), recalling that these species are characteristic of Cu–CZ interface sites and are proposed to be formed by a CO-induced $Cu^{2+} \rightarrow Cu^{+}$ reductive interaction which is energetically very favored in this type of system (38), and a subsequent CO adsorption on the reduced site (26, 27). On the other hand, on the basis of the slower growth of Pd^0 carbonyls with increasing reaction temperature observed for the bimetallic system (Fig. 6C), the existence of a copper-induced blocking effect, hindering the establishment of Pd–CZ interactions, is supported by the fact that Pd reduction under reaction conditions appears somewhat retarded for PdCuCZ with respect to PdCZ (data obtained under similar conditions presented in (21)). Nevertheless, a certain specific role of Pd on the catalytic activity of this catalyst is inferred from comparative analysis of the catalytic performances of CuCZ and PdCuCZ (Table 2). This may be related either to Pd-assisted CO activation for further reaction on the Cu–CZ sites or, more simply, to the fact that the blocking effect is only partial with some Pd–CZ contacts remaining in the catalyst. As discussed in Section 4.3, a combined analysis of catalytic performance for CO–O_2 and CO–O_2–NO reactions suggests the former as the more likely hypothesis. In any case, one cannot fully dismiss the fact that the peculiar catalytic behavior observed for PdCuCZ is related to the formation of a certain Cu-enriched Pd–Cu alloy with limited catalytic activity; in this respect, experiments are in progress which should provide a more complete picture of the Pd state in this catalyst (39).

The presence of alumina appears to play an important role in the copper-promoting effects observed for the PdCuxCZA catalysts. This is most likely related to the fact, according to EPR results (Fig. 4), that copper appears to interact preferentially with the alumina component and could induce different effects on the active Pd species. On the one hand, this may lead to a relative increase in the amount of Pd–3D-CZ active sites by simply decreasing, by a blocking effect, the number of sites available on the alumina for Pd deposition during sample preparation. A comparison of XEDS values for Pd in these catalysts (Fig. 3) to similar data reported for the PdxCZA catalysts (21) is not conclusive in this respect. On the other hand, XANES results which indicate the formation of a Pd–Cu alloy (Fig. 10) suggest that the main effect induced by the affinity of copper for establishing interactions with the alumina component can be related to facilitating the formation of an active Pd–Cu alloy in contact with 3D-CZ entities by decreasing the copper concentration in that alloy. According to previous work, promoting effects for CO oxidation induced upon alloy formation are related to a greater stabilization of the zero-valent state of Pd (18). A comparison between XANES experiments under CO–O_2–NO for PdCu33CZA (Fig. 10) and Pd33CZA (10) supports this hypothesis, as a somewhat lower temperature is required for Pd reduction in the bimetallic system. In any case, the higher activity of PdCu33CZA with respect to PdCu10CZA can be related to the greater amount of (Cu–)Pd–3D-CZ contacts present in the former (21), as suggested by XEDS results (Fig. 3). In terms of mechanistic aspects for this reaction, DRIFTS

results indicate that the PdCuxCZA systems behave in a similar manner to their homologous PdxCZA systems (21), thus indicating that CO and O_2 are activated at metallic Pd and $V_{ö}$ sites of CZ located at the metal–CZ interface, following a reaction path that overcomes the CO-inhibition effects present in the absence of the mixed oxide promoter (30).

4.3. Catalytic Activity for the CO–O_2–NO Reaction

When comparing CO oxidation activity in this reaction, analysis of the reactivity profiles for CO oxidation in the presence and absence of NO (Fig. 5 and Table 2) reveals that the effect induced on each of the samples by the presence of NO in the reactant mixture essentially depends on whether alumina is present or absent. While PdCuxCZA samples are apparently deactivated, PdCuCZ is almost insensitive to the presence of NO. NO-induced deactivation effects for CO oxidation over PdCuxCZA catalysts can be related in the main to the greater difficulty in achieving the active Pd^0 states in the presence of NO, as proposed previously for the reference PdxCZA catalysts (10). This is apparent from comparisons of the intensities of Pd^0-adsorbed carbonyls between DRIFTS experiments of Figs. 6 and 8 and has been related to an NO-induced stabilization of oxidized states of Pd, as evidenced by the relatively greater stability of the Pd^{2+}-carbonyl species which give the band at 2158–2155 cm^{-1}, either under reaction conditions (compare Figs. 6 and 8) or in postreaction experiments (compare Figs. 7 and 9). This has been shown to affect the Pd–(3D-CZ) active sites for the reaction (10, 21).

The absence of the Pd^{2+}-carbonyl band at 2158–2155 cm^{-1} for PdCuCZ in the presence of NO, which is in strong contrast to similar experiments performed on PdCZ (10), further evidences the absence of Pd–CZ interactions in that sample. As indicated earlier and in accordance with the similar behavior observed for CuCZ (Table 2), the insensitivity of CO oxidation activity to the presence of NO can be related to the Cu–CZ interfacial nature of the active sites in PdCuCZ. The observation of significant amounts of NO desorbed at low reaction temperatures for PdCuCZ (Fig. 5, bottom) correlate well with the presence and evolution at the reaction temperature of adsorbed nitrosyl species on Cu^{2+} (Fig. 8C). These results also concur with those obtained for CuCZ (40). On the other hand, the fact that the Cu^{+}-carbonyl band observed for PdCuCZ is of appreciably lower intensity and appears slightly blue-shifted in the presence of NO at the lower reaction temperatures (compare Figs. 6C and 8C) suggests that copper at Cu–CZ sites is less readily reduced when NO is present, with the blue shift being related to the higher average oxidation state of the oxidic copper environment surrounding the Cu^{+}-carbonyl species (23, 41, 42). It is interesting that this NO-induced oxidizing interaction affecting active copper species does not modify the CO oxidation activity of the PdCuCZ system. This may be related, recalling previous work (26), to the fact that the rate-determining step for that reaction over CuCZ was attributed to the oxidizing steps (related to O_2 reduction) within a redox mechanism in which CO oxidation and O_2 reduction processes are competing. These steps were related to the processes of oxidation of $V_{ö}$ sites of the CZ component, which would not be significantly affected by interaction with NO. Experiments are in progress to further elucidate these aspects (40).

Results for all catalysts show a copper-promoting effect on the CO oxidation reaction in a CO–O_2–NO mixture (Table 2). In the case of the PdCuCZ this may be attributed to the particular properties of the Cu–CZ active sites along with a certain contribution of Pd (Table 2), probably related to its participation in CO activation processes. For the

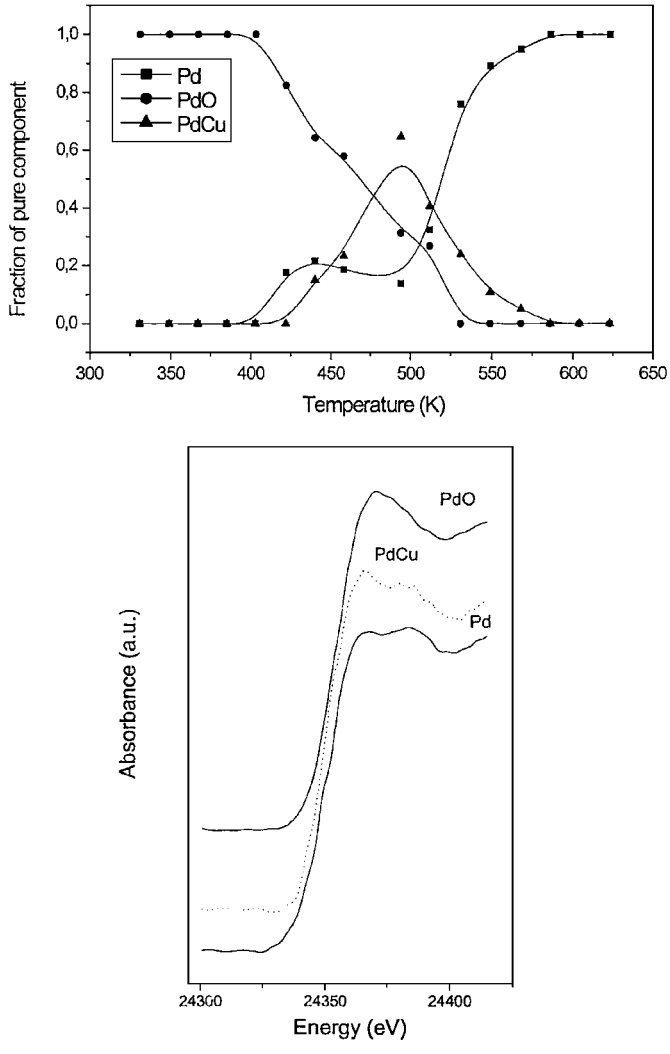

FIG. 10. Top: Evolution of individual components as a function of the reaction temperature in the *in situ* XANES spectra at the Pd K-edge of PdCu33CZA. Bottom: Individual components obtained through analysis of the Pd K-edge XANES spectra.

PdCuxCZA catalysts, the promoting effect may be attributed to the beneficial properties of alloy formation. It must be noted from DRIFTS and XANES experiments (Figs. 8 and 10) that Pd reduction is first produced at a surface level which occurs at 303 K immediately upon contact between the catalyst and the reactant mixture (Fig. 8), while progress of the reduction into the bulk of the particles is produced at $T \geq 403$ K (Fig. 10).

The lack of copper-related promoting effects for NO reduction in the PdCuxCZA systems, which differs from results for a 10 wt% CeO_2/Al_2O_3-supported Pd–Cu catalyst (18), may be attributed, according to XANES evidence (Fig. 10), to the destruction of the alloy phase below the temperature at which NO activation is achieved. This may result in a more heterogeneous situation in the catalysts in which the detrimental effects of the presence of small amounts of alloy-derived copper, at metal–CZ interface sites (as proposed to occur for PdCuCZ), may lead to a small degree of deactivation for that reaction (in accordance with the lower activity shown by CuCZ, Table 2). The destruction of the alloy in these catalysts is intriguing when considering the greater thermodynamic stability of that phase with respect to the individual metals (18). It may be noted that a comparison to a Pd–Cu/CeO_2/Al_2O_3 catalyst treated under similar conditions, which showed a high stability for the generated Pd–Cu alloy (18), suggests that alloy destruction in the CZ-based systems may be related to the high stability of copper in the zirconia phase.

CONCLUSIONS

The effects of copper on the catalytic behavior of a series of bimetallic Pd–Cu catalysts supported on (Ce,Zr)O_x or (Ce,Zr)O_x/Al_2O_3 supports (prepared by a reverse microemulsion method) for CO oxidation–NO reduction under CO–O_2 or CO–O_2–NO stoichiometric mixtures are proposed to depend strongly on the metal distribution over each of the supports. XRD and TEM–XEDS techniques were used to characterize the mixed oxide component showing the formation of Ce–Zr mixed oxide nanoparticles with Ce/Zr ratios close to the nominal value of 1 and in which a certain degree of structural heterogeneity and a small enrichment in Ce are observed for the Al_2O_3-supported sample with the higher (Ce,Zr)O_x loading (33 wt%). Differences in the distributions of the two metallic components over the different supports were demonstrated by XEDS and EPR spectroscopies and by catalytic activity results.

To rationalize the catalytic behavior of the samples, they can be classified into two groups as a function of the presence or absence of alumina in the support.

1. The catalytic behavior of Pd–Cu/(Ce,Zr)O_x is explained by the particular nature of its active sites which is constituted by contacts between copper and mixed oxide, with palladium having a more limited role, and attributed to a certain participation in the CO-activation processes. This is based on the following catalytic or spectroscopic evidence: (i) As occurs for a Cu/(Ce,Zr)O_x reference sample, catalytic activity for CO oxidation is almost insensitive to the presence of NO. (ii) The presence of Cu–(Ce,Zr)O_x interface sites is revealed by the formation of Cu^+-carbonyl species (IR band at 2110 cm^{-1}) characteristic of these sites (27). (iii) The absence of contacts between Pd and support is indicated not only by the slower thermal reduction of Pd under reaction conditions in comparison to a Pd/(Ce,Zr)O_x reference sample (21) but also by the lack of formation of Pd^{2+} carbonyls at low reaction temperatures in the presence of NO. These latter carbonyl species are characteristic of Pd–(Ce,Zr)O_x sites and were presented as the main evidence in explaining NO-induced deactivating effects for CO oxidation in the monometallic Pd series of catalysts (10).

2. In Pd–Cu/(Ce,Zr)O_x/Al_2O_3 samples; copper-promoting effects for CO oxidation (with either O_2 or O_2–NO mixtures) are attributed to the formation of a Pd–Cu alloy (evidenced by *in situ* XANES) in contact with the Ce–Zr mixed oxide component. The achievement of optimum properties for the Pd–Cu alloy is proposed to be favored by a preferential interaction between copper and alumina, probably leading to a decrease in the copper concentration of the alloy phase. The destruction of the alloy under reaction conditions at high temperatures required for NO activation is proposed as the main cause for the absence of copper-promoting effects for NO reduction in these systems.

ACKNOWLEDGMENTS

A. B. Hungria, A. Iglesias-Juez, and A. Martinez-Arias thank the Comunidad de Madrid for grants received with which this work has been carried out and for financial assistance (to A. Martinez-Arias) under the "Ayudas para estancias breves en centros de investigación extranjeros" program. Thanks are due to the scientific and technical staff at LURE Synchrotron for their help during the XANES experiments. Financial help by CICYT (Project MAT2000-1467) is also acknowledged.

REFERENCES

1. Lox, E. S. J., and Engler, B. H., *in* "Environmental Catalysis" (G. Ertl, H. Knözinger, and J. Weitkamp, Eds.), p. 1. Wiley-VCH, Weinheim/New York, 1999.
2. Trovarelli, A., *Catal. Rev. Eng. Sci.* **38**, 97 (1996) and references therein.
3. Lafyatis, D. S., Ansell, G. P., Bennett, S. C., Frost, J. C., Millington, P. J., Rajaram, R. R., Walker, A. P., and Ballinger, T. H., *Appl. Catal. B* **18**, 123 (1998).
4. Kašpar, J., Fornasiero, P., and Graziani, M., *Catal. Today* **50**, 351 (1999).
5. Jiang, J. C., Pan, X. Q., Graham, G. W., McCabe R. W., and Schwank, J., *Catal. Lett.* **53**, 37 (1998).
6. Martínez-Arias, A., Fernández-García, M., Ballesteros, V., Salamanca, L. N., Otero, C., Conesa, J. C., and Soria, J., *Langmuir* **15**, 4796 (1999).
7. Fernández-García, M., Martínez-Arias, A., Iglesias-Juez, A., Belver, C., Hungría, A. B., Conesa, J. C., and Soria, J., *J. Catal.* **194**, 385 (2000).

8. Yao, M. H., Blaird, N. J., and Kunz, F. W., *J. Catal.* **166**, 67 (1997).
9. Ozawa, M., Matuda, K., and Suzuki, S., *J. All. Comp.* **303–304**, 56 (2000).
10. Martínez-Arias, A., Fernández-García, M., Iglesias-Juez, A., Hungría, A. B., Anderson, J. A., Conesa, J. C., and Soria, J., *Appl. Catal. B* **31**, 51 (2001).
11. Di Monte, R., Fornasiero, P., Kašpar, J., Graziani, M., Gatica, J. M., Bernal, S., and Gómez-Herrero, A., *Chem. Commun.* 2167 (2000).
12. van Yperen, R., Lindner, D., Mubmann, L., Lox E. S., and Kreuzer, T., *Stud. Surf. Sci. Catal.* **116**, 51 (1998).
13. Hu, Z., Wan, C. Z., Lui, Y. K., Dettling, J., and Steger, J. J., *Catal. Today* **30**, 83 (1996).
14. Skoglundh, M., Johansson, H., Löwendahl, L., Jansson, K., Dahl, L., and Hirschauer, B., *Appl. Catal. B* **7**, 299 (1996).
15. Taylor, K. C., *Catal. Rev. Sci. Eng.* **35**, 457 (1993).
16. Trillat, J. F., Massadier, J., Morawek, B., Praliaud, H., and Renouprez, A. J., *Stud. Surf. Sci. Catal.* **116**, 103 (1998).
17. El Hamdaoui, A., Bergeret, G., Massadier, J., Primet, M., and Renouprez, A. J., *J. Catal.* **148**, 47 (1994).
18. Fernández-García, M., Martínez-Arias, A., Belver, C., Anderson, J. A., Conesa, J. C., and Soria, J., *J. Catal.* **190**, 387 (2000).
19. Fernández-García, M., Conesa, J. C., Clotet, A., Ricart, J. M., López, N., and Illas, F., *J. Phys. Chem. B* **102**, 141 (1998).
20. Fernández-García, M., Martínez-Arias, A., Anderson, J. A., Conesa, J. C., and Soria, J., *Stud. Surf. Sci. Catal.* **130**, 1325 (2000).
21. Fernández-García, M., Martínez-Arias, A., Iglesias-Juez, A., Hungría, A. B., Anderson, J. A., Conesa, J. C., and Soria, J., *Appl. Catal. B* **31**, 39 (2001).
22. Márquez-Alvarez, C., Rodríguez-Ramos, I., Guerrero-Ruiz, A., Haller, G. L., and Fernández-García, M., *J. Am. Chem. Soc.* **119**, 2905 (1997).
23. Martínez-Arias, A., Cataluña, R., Conesa, J. C., and Soria, J., *J. Phys. Chem. B* **102**, 809 (1998).
24. Berger, P. A., and Roth, J. F., *J. Phys. Chem.* **71**, 4307 (1967).
25. Tavares Figueiredo, R., Martínez-Arias, A., López Granados, M., and Fierro, J. L. G., *J. Catal.* **178**, 146 (1998).
26. Martínez-Arias, A., Fernández-García, M., Gálvez, O., Coronado, J. M., Anderson, J. A., Conesa, J. C., Soria, J., and Munuera, G., *J. Catal.* **195**, 207 (2000).
27. Martínez-Arias, A., Fernández-García, M., Soria, J., and Conesa, J. C., *J. Catal.* **182**, 367 (1999).
28. Martínez-Arias, A., Soria, J., Cataluña, R., Conesa, J. C., and Cortés Corberán, V., *Stud. Surf. Sci. Catal.* **116**, 591 (1998).
29. Fernández-García, M., Martínez-Arias, A., Salamanca, L. N., Coronado, J. M., Anderson, J. A., Conesa, J. C., and Soria, J., *J. Catal.* **187**, 474 (1999).
30. Xu, X., and Goodman, D. W., *J. Phys. Chem.* **97**, 7711 (1993).
31. Bensalem, A., Muller, J. C., Tessier, D., and Bozon-Verduraz, F., *J. Chem. Soc., Faraday Trans.* **92**, 3233 (1996).
32. Anderson, J. A., Márquez-Alvarez, C., López-Muñoz, M. J., Rodríguez-Ramos, I., and Guerrero-Ruiz, A., *Appl. Catal. B* **14**, 189 (1997).
33. Hall, W. K., and Vaylon, J., *Catal. Lett.* **15**, 311 (1992).
34. Hierl, R., Urbach H.-P., and Knözinger, H., *J. Chem. Soc., Faraday Trans.* **88**, 355 (1992).
35. Fernández-García, M., Gómez Rebollo, E., Guerrero Ruiz, A., Conesa, J. C., and Soria, J., *J. Catal.* **172**, 146 (1997).
36. Fernández-García, M., Anderson, J. A., and Haller, G. L., *J. Phys. Chem.* **100**, 16,247 (1996).
37. Mehran, F., Barnes, S. E., Chandrashekar, G. V., McGuire, T. R., and Shafer, M. W., *Solid State Commun.* **67**, 1187 (1988).
38. Bera, P., Mitra, S., Sampath S., and Hedge, M. S., *Chem Commun.* 927 (2001).
39. Fernández-García, M., Martínez-Arias, A., Iglesias-Juez, A., Hungría, A. B., Anderson, J. A., Conesa, J. C., and Soria, J., in preparation.
40. Martínez-Arias, A., Fernández-García, M., Hungría, A. B., Gálvez, O., Anderson, J. A., Soria, J., Conesa, J. C., and Munuera, G., in preparation.
41. Padley, M. B., Rochester, C. H., Hutchings G. J., and King, F., *J. Catal.* **148**, 438 (1994).
42. Lokhov, Y. A., Sadykov, V. A., Tikhov, S. F., and Popovskii, V. V., *Kinet. Katal.* **26**, 177 (1985).